RSC Advances

ROYAL SOCIETY OF CHEMISTRY

PAPER

View Article Online
View Journal | View Issue

Check for updates

Cite this: *RSC Adv.*, 2021, **11**, 14475

Evaluation of $BaCo_{0.4}Fe_{0.4}Zr_{0.2-x}Ni_xO_{3-\delta}$ perovskite cathode using nickel as a sintering aid for IT-SOFC

Muneeb Irshad, *[a] Mehak Khalid,[a] Muhammad Rafique,[b] Naveed Ahmad,[c] Khurram Siraj,[a] Rizwan Raza, [de] Muhammad Sadiq,[a] Muhammad Ahsan,[f] Abdul Ghaffar[g] and Amina Ashfaq[a]

Received 29th January 2021
Accepted 8th April 2021

DOI: 10.1039/d1ra00789k

rsc.li/rsc-advances

In this research work, $BaCo_{0.4}Fe_{0.4}Zr_{0.2-x}Ni_xO_{3-\delta}$ ($x = 0, 0.01, 0.02, 0.03, 0.04$) perovskite cathode material for IT-SOFC is synthesized successfully using a combustion method and sintered at low temperature. The effects of nickel as a sintering aid on the properties of $BaCo_{0.4}Fe_{0.4}Zr_{0.2}O_{3-\delta}$ are investigated through different characterization methods. The addition of nickel increased the densification and grain growth at a lower sintering temperature 1200 °C. XRD analysis confirms a single phase of $BaCo_{0.4}Fe_{0.4}Zr_{0.2}O_{3-\delta}$, and an increase in crystalline size is observed. SEM micrographs show formation of dense microstructure with increased nickel concentration. TGA analysis revealed that $BaCo_{0.4}Fe_{0.4}Zr_{0.2-x}Ni_x$ cathode materials are thermally stable within the SOFC temperature range, and negligible weight loss of 2.3% is observed. The bonds of hydroxyl groups and metal oxides are confirmed for all samples through FTIR analysis. The highest electrical properties are observed for $BaCo_{0.4}Fe_{0.4}Zr_{0.2-x}Ni_x$ ($x = 0.04$) due to increased densification and electronic defects compared to other compositions. The maximum power density of 0.47 W cm^{-2} is obtained for a cell having cathode material $BaCo_{0.4}Fe_{0.4}Zr_{0.2-x}Ni_x$ ($x = 0.02$) owing to its permeable and well-connected structure compared to others.

1 Introduction

In the last decade, rapid urbanization and industrialization along with population growth have led to an exponential increase in energy demand. Traditional energy resources like coal, gas, and petroleum are used to fulfill humankind's energy needs. The extensive use of these energy resources is not only creating a negative impact on the environment by the emission of harmful gases but also causing their depletion at a rapid pace.[1,2] Researchers are devoting a lot of their efforts to develop highly efficient, cost-effective, and eco-environment-friendly alternative energy resources. Among different energy resources, fuel cells have the potential in fulfilling these requirements. The solid oxide fuel cell (SOFC), among other types, is mostly preferred owing to its elevated energy conversion efficiency, inherent simplicity, less noise, fuel diversity, and insignificant by-products.[3,4] The drawback of SOFC is its high operating temperature which causes little chemical stability leading to high maintenance and production cost.[5] High temperature also causes a thermal mismatch with other components. However, SOFC operating temperature significantly decreased (from 1000 °C to 400 °C) in the past decade, by developing new and innovative materials without affecting their conductivity. However, efforts are still needed to create materials that can further reduce its operating temperature.[6–8]

In SOFC, cathode must have adequate porosity and high electronic conductivity for better oxygen reduction reaction (ORR).[9] At the cathode, the overall molecule used for the electrochemical reaction is O_2 (diatomic species) and it converts into an electro-active ion through one or more processes, and this reaction typically occurs near the TPBs.[10] Micro-pattern and composition of materials used for electrolyte and cathode can also influence the TPB aspects and distribution.[11,12]

Recently perovskite cathode materials gained significant importance due to their considerable oxide ion conductivity and excellent electronic conductivity, makes them mixed ionic-electronic conductors and have great significance as cathode material.[13,14] Perovskite has the formula $ABO_{3\pm\delta}$, where δ indicates the excess or deficiency of the oxygen, and A-cation is a metal with charge +2 or +3 larger than B-cation having charge

---

[a] Department of Physics, University of Engineering and Technology, Lahore, 54890, Pakistan. E-mail: muneebirshad@gmail.com

[b] Department of Physics, University of Sahiwal, Sahiwal, Pakistan

[c] Department of Physics, University of Education, Township, Lahore, Pakistan

[d] Clean Energy Research Lab (CERL), Department of Physics, COMSATS University Islamabad, Lahore Campus, Lahore, 54000, Pakistan

[e] Department of Physics, Chemistry, and Biology, Semiconductor Materials, Linköping University, Sweden

[f] Department of Thermal Power and Energy Engineering, Huazhong University of Science and Technology, China

[g] Department of Physics, Government College University, Lahore, Pakistan

+4 or +3. The positive valances of A and B cations are six and exist as "$A^{2+}B^{4+}O_3$, $A^{1+}B^{5+}O_3$ or $A^{3+}B^{3+}O_3$". Electrical conductivity and electrocatalytic performance of perovskites cathode material can be enhanced by using dopants at A and B sites of the structure.[15] In perovskite cathode materials, the A site is comprised of the rare and alkaline earth metals that is La, Ba, Ca, or Sr, while B site consists of transition metals such as Mn, Ni, Co, or Fe, *etc.* B-site cations, therefore, give the catalytic mechanism.[16] Barium zirconate and barium cerate both have perovskite structures. Barium cerate as a perovskite material is preferred because of its high storage capacity of oxygen vacancies and high conductivity compared to barium zirconate.[17]

The perovskites cathode material doped with rare-earth elements like Sr, Ce, and Co, *etc.*, have shown tremendous advantages over conventional cathodes.[14] These cathode materials provide better matching thermo-mechanical performance with electrolytes and show mixed ionic and electronic conductivity.[18,19] Therefore, perovskite-type MIECs having a composition of ABO_3 are best for oxygen permeability because of their excellent ionic and electronic conductivity over a different range of temperature.[20] Cobalt-based perovskite material is the most suitable material in the family of MIEC materials. The substitution in cobalt-based perovskite structure from A or B site helps obtain materials that have good structural stability and high oxygen permeability.

To use a sintering aid, it is crucial that dopant can increase the point defects, and it can also enhance the transportation of ions or electrons to promote sintering.[21,22] Nickel is considered as to be fast diffuser and it enhances the sintering rate of the ceramic powders. It was also reported that during sintering the addition of nickel suppresses the coarsening process of grains to some extent.[23] The substitution of nickel in BCFZ not only helps in reducing the sintering temperature but it also increases the oxygen concentration and permeability at an intermediate temperature which is favourable for the transportation of O_2 ions in bulk electrode, therefore resulting into enhanced electrocatalytic performance. Furthermore, it also reduces the reactivity of the electrolyte with the cathode and lead to the excellent performance of the SOFC.[24]

In current work, nickel is used as a sintering aid in BCFZ to observe the effect of sintering aid on sintering temperature, crystal structure, surface morphology, grain size and shape, temperature effects, conductivity, and electrochemical performance. A series of $BaCo_{0.4}Fe_{0.4}Zr_{0.2-x}Ni_xO_{3-\delta}$ ($x = 0, 0.01, 0.02, 0.03, 0.04$) perovskite cathode materials were synthesized through cost and time effective auto-combustion method.

2 Experimentation of samples

$BaCo_{0.4}Fe_{0.4}Zr_{0.2-x}Ni_xO_{3-\delta}$ ($x = 0, 0.01, 0.02, 0.03, 0.04$) perovskite cathode materials were synthesized through auto-combustion method for IT-SOFC. The precursor materials used for the synthesis of $BaCo_{0.4}Fe_{0.4}Zr_{0.2-x}Ni_xO_{3-\delta}$ were Ba$(NO_3)_3$ (Sigma Aldrich, > 98%), $Co(NO_3)_2 \cdot 6H_2O$ (Sigma Aldrich, > 98%), $Ni(NO_3) \cdot 6H_2O$ (Sigma Aldrich, > 98%), $Zr(NO_3)_4 \cdot 5H_2O$ (Sigma Aldrich, > 98%) and $Fe(NO_3)_2 \cdot 9H_2O$ (Sigma Aldrich, > 98%). The homogenous solution was prepared by adding a stoichiometric amount of these materials in de-ionized water under constant stirring and heating at 80 °C. Oxalic acid as a chelating agent was used for auto combustion. The obtained solution was then continuously stirred and heated at 120 °C until gel formation took place. The gel was then placed within the oven at 120 °C for auto ignition, and $BaCo_{0.4}Fe_{0.4}Zr_{0.2-x}Ni_x$ cathode powder was obtained, which was sintered at 1200 °C for 4 hours. The fine powder was obtained through grinding. Pellets of $BaCo_{0.4}Fe_{0.4}Zr_{0.2-x}Ni_xO_{3-\delta}$ powder were prepared by the hydraulic press at a pressure of 300 MPa.

Different characterization techniques were employed to observe the structural improvement of BCFZ perovskite cathode material cells using NiO as a sintering aid. XRD was used for structural analysis, and crystallite size was determined using the Scherer equation. The surface morphology of synthesized cathode materials was observed through SEM (HITACHI S-3000H). Weight loss was followed by thermo-gravimetric analysis (TGA Q500). FTIR analysis was used to investigate the functional groups and presence of metal oxide in the cathode material. Four probe DC methods were employed to determine the conductivities of the samples. The relation between conductivity and temperature was determined by the Arrhenius equation given by,[25]

$$\sigma = \frac{A}{T}\exp\left(-\frac{E_a}{KT}\right) \tag{1}$$

The electrochemical performance is evaluated by fabricating five anode supported button cells having configuration $BaCo_{0.4}Fe_{0.4}Zr_{0.2-x}Ni_xO_{3-\delta}$/SDC/Ni-SDC. The cathode slurry was printed on the SDC and was calcined at 1000 °C for 4 hours. Each button cell is prepared in the form circular disk with a diameter of 16 mm and thickness of 0.5 mm. The silver paste is used on both cathode and anode to collect current and is then treated at 500 °C for 1 hour. The humidified hydrogen (~3% H_2O) is provided at the anode as a fuel with a flow rate of 50 mL min^{-1}, and at cathode, ambient air as an oxidant is used.

3 Result and discussion

3.1 Surface morphology

Fig. 1(a–e) shows the SEM micrographs of $BaCo_{0.4}Fe_{0.4}Zr_{0.2-x}Ni_xO_{3-\delta}$ cathode materials. It is clear from the micrographs that $BaCo_{0.4}Fe_{0.4}Zr_{0.2-x}Ni_xO_{3-\delta}$ structure becomes dense and less porous with increased content of nickel. Composition ($x = 0$) shows the least dense structure while composition ($x = 0.04$) shows the most dense structure. It can be deduced from SEM micrographs that pores reduced because nickel melted during sintering and diffused into the lattice of host Zr^{4+}, and it also acted as a sintering aid due to its high surface energy.[26] The increased concentration of Ni in $BaCo_{0.4}Fe_{0.4}Zr_{0.2-x}Ni_xO_{3-\delta}$ also resulted into increased particle size and agglomeration which lead to further densification and grain growth.[27,28] $BaCo_{0.4}Fe_{0.4}Zr_{0.2-x}Ni_xO_{3-\delta}$ for ($x = 0.01, 0.02$) exhibit moderate porous structure and well-connected network along with increased TPB compared to other compositions, which is favorable for the enhanced electrochemical performance of cathode.[29] It can also be deduced from these micrographs that microstructures of $BaCo_{0\cdot4}Fe_{0\cdot4}Zr_{0.2-x}Ni_xO_{3-\delta}$ cathode materials became more compact and less permeable even at 1200 °C. Therefore, for these compositions, the sintering temperature can be further lowered to avoid agglomeration and to obtain porous and well-connected structures. The lowering of sintering temperature will make the synthesis process more cost-effective.[30] The SEM analysis validates the fact that NiO played its role as a sintering aid and resulted in increased densification of BCFZ at much lower sintering temperatures.

3.2 Structural study

Fig. 2 represents the XRD spectra of $BaCo_{0\cdot4}Fe_{0\cdot4}Zr_{0.2-x}Ni_xO_{3-\delta}$ cathode materials within a 2θ range of 20°-70°. Single-phase perovskite planes (210), (111), (002), (110), (114), (400), (−322) and (003) are observed for all samples (JCPDS 75-0227, BCFZ). The sintering temperature is an important factor for the formation of perovskite phases because doped and undoped material shows the same crystal structure.[31] The dominant phases before doping were monoclinic due to the zirconia, whereas doping of a small amount of nickel oxide suppressed the monoclinic structure and tetragonal phases get enhanced.[32] Defect chemistry and the hydroxylation degree are the main aspects that dominate the properties of tetragonal structure of ZrO_2. The phase change and stability of tetragonal phase is strongly dependent upon the dopant used. In the current work, the formation of the tetragonal phase depends upon the concentration of the nickel added. The small particle size of the nickel compared to the zirconia increases the reactivity and led to the stabilization of the tetragonal phase. The addition of nickel suppresses the monoclinic phases and enhances the tetragonal phase.[33] It can be further deduced that after doping of nickel up to 4 mol%, the perovskite structure remains intact, which is also in agreement with the reported results. However, the secondary phase of BaO is observed for all samples while the NiO phase is observed for $BaCo_{0\cdot4}Fe_{0\cdot4}Zr_{0.2-x}Ni_xO_{3-\delta}$. The existence of BaO phase can be ascribed to low sintering temperature as researchers have reported that high sintering temperature can result in the volatilization of BaO.[1]

It is also clear from the spectra that besides the NiO phase's appearance due to nickel, peak shifting also occurred for the samples doped with nickel. Fig. 3 represents the peak shifting of the (210) plane of $BaCo_{0\cdot4}Fe_{0\cdot4}Zr_{0.2-x}Ni_xO_{3-\delta}$. It can be observed that plane moved to a higher angle with an increased ratio of nickel. The increased concentration of nickel within $BaCo_{0\cdot4}Fe_{0\cdot4}Zr_{0.2-x}Ni_xO_{3-\delta}$ disturbed the perovskite structure symmetry due to disparity in the ionic radii of host and dopant that resulted in peak shifting towards the higher angle.[34] The shifting toward a higher angle can be ascribed to the small ionic radius of Ni^{2+} ions (1.62 Å) compared to Ba^{2+} (2.78 Å) and Zr^{4+} (2.16 Å) that resulted in the shrinkage of lattice parameter and led to a decreased unit cell.[35]

XRD spectra further reveal that the intensity of peaks increased with the augmented concentration of nickel because nickel improved the sinterability of $BaCo_{0\cdot4}Fe_{0\cdot4}Zr_{0.2-x}Ni_xO_{3-\delta}$.[36] When NiO doped at B-position in the perovskite structure, there is a reduction of oxygen vacancies which resulted in shrinkage of lattice and increased the intensity of the peaks.

The crystallite size was determined by the Debye–Scherrer formula.[35]

$$D = \frac{K\lambda}{\beta \cos \theta} \tag{2}$$

Table 1 shows that crystallite size increased with increased concentration of nickel which can be attributed to an increase in grain growth and aggregation. The increased concentration of nickel resulted in increased nucleation of crystallites and enhanced grain growth. Earlier reported results also confirm the same behavior when nickel is used as sintering aid.[37,38]

3.3 FTIR analysis

Fig. 4 shows the FTIR transmittance spectra of $BaCo_{0\cdot4}Fe_{0\cdot4}Zr_{0.2-x}Ni_xO_{3-\delta}$ cathode material in a range of 4000–600 cm^{-1}.

The peaks around 1600 cm^{-1} show N–H bindings due to the amines group, while peaks at 1400 cm^{-1} represent the C–C stretching in the rings due to aromatics compounds and water adsorption.[39] These peaks get broader with increased concentration of nickel in $BaCo_{0\cdot4}Fe_{0\cdot4}Zr_{0.2-x}Ni_xO_{3-\delta}$. Peak shifting is also observed, which can be attributed to the shrinkage of lattice parameter, decreased unit cell volume, and trapping effects of charges between host Zr^{4+} and nickel dopant.[40] The shifting of peaks can also be related to the structural disorder and stresses that are produced due to the difference in ionic radii dopant Ni and host Zr^{4+}, therefore, resulting in displacement and tilting of zirconium oxide structure.[41] Stability and structure disorder are inversely proportional to each other.[42] Also due to this difference, the metal oxide bonds which change the internal motion of molecules, resulted in increased bond length for cathode materials.[43,44]

3.4 Thermal analysis

Fig. 5 shows the TGA plot of $BaCo_{0\cdot4}Fe_{0\cdot4}Zr_{0\cdot2x}N_xO_{3-\delta}$ in a range from room temperature to 850 °C. A minimal weight loss of about 2.3% is observed from 100 °C to 140 °C approximately. This weight loss is due to the evaporation of water present within the sample due to ambient moisture. No weight loss is observed beyond 140 °C because the thermal analysis is done after sintering; therefore, metal nitrates and residual compounds were already decomposed. It is also clear that no thermal process decomposition or evaporation occurred within the SOFC operating temperature range, which depicts that it is thermally stable for SOFC operating temperature.[45]

3.5 Conductivity

Fig. 6 depicts the Arrhenius plot between ln σT and $1/T$ for $BaCo_{0\cdot4}Fe_{0\cdot4}Zr_{0.2-x}Ni_xO_{3-\delta}$ cathode material within the temperature range of 500–900 °C.

It can be observed from the figure that electronic conductivity increased with the increased concentration of NiO. When

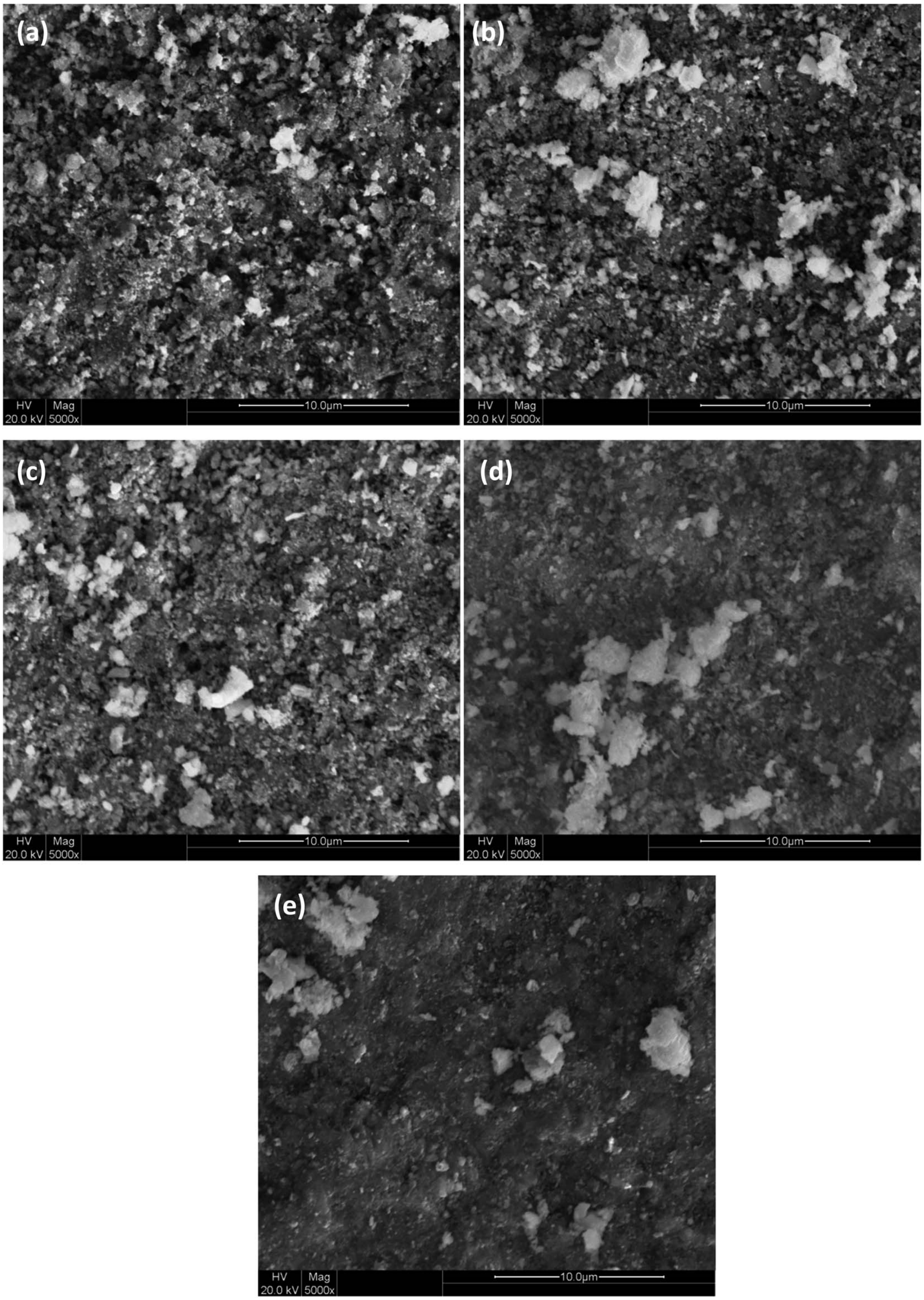

Fig. 1 Surface morphology of $BaCo_{0\cdot4}Fe_{0\cdot4}Zr_{0.2-x}Ni_xO_{3-\delta}$, x = (a) 0, (b) 0.01, (c) 0.02, (d) 0.03 and (e) 0.04.

NiO doped by decreasing the zirconium concentration, the ions of zirconium reduced in host $BaCo_{0\cdot4}Fe_{0\cdot4}Zr_{0.2-x}Ni_xO_{3-\delta}$, which produces distortion in the lattice of host materials.[46]

The materials' conductivity depends upon two parameters mobility of charge carriers and their concentration.[47] Charge carriers mainly depend upon occupied and available sites. They are also dependent upon the energy gap and grain shape obtained after the sintering process.[25] Porosity reduces, and grain size increases at higher sintering temperatures resulting in increased charge carriers' fraction.[48,49] For metal oxide cathodes, there is molecular oxygen adsorption, and diffusion at the surface of the electrode, and oxygen ions transfer from TPB to

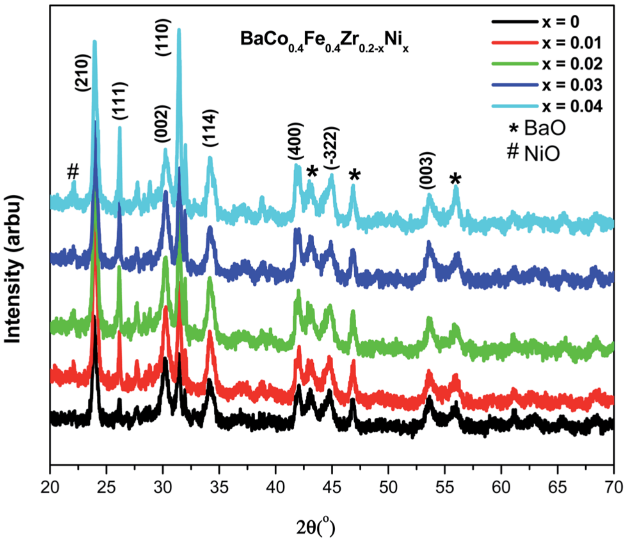

Fig. 2 XRD spectra of $BaCo_{0.4}Fe_{0.4}Zr_{0.2-x}Ni_xO_{3-\delta}$.

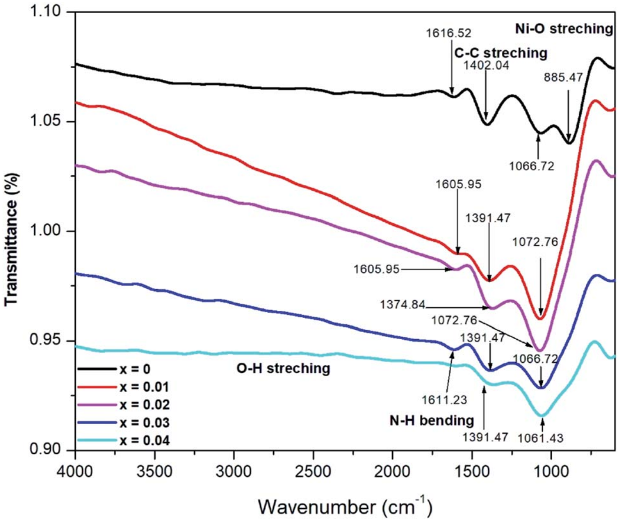

Fig. 4 FTIR spectra of $BaCo_{0.4}Fe_{0.4}Zr_{0.2-x}Ni_xO_{3-\delta}$.

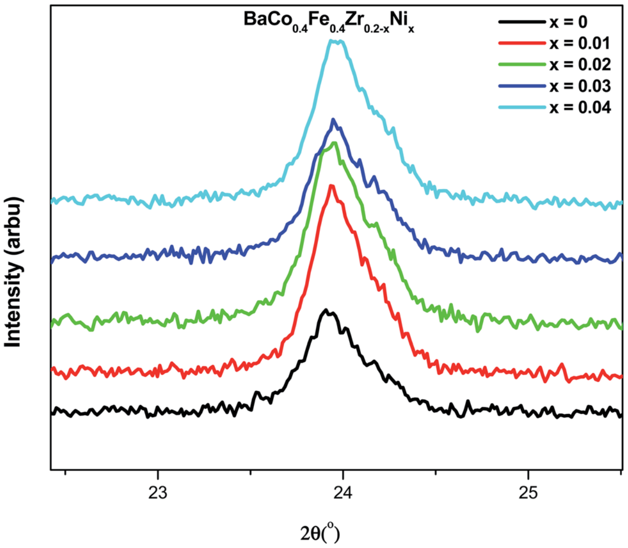

Fig. 3 Magnified plane (210) peak $BaCo_{0.4}Fe_{0.4}Zr_{0.2-x}Ni_xO_{3-\delta}$.

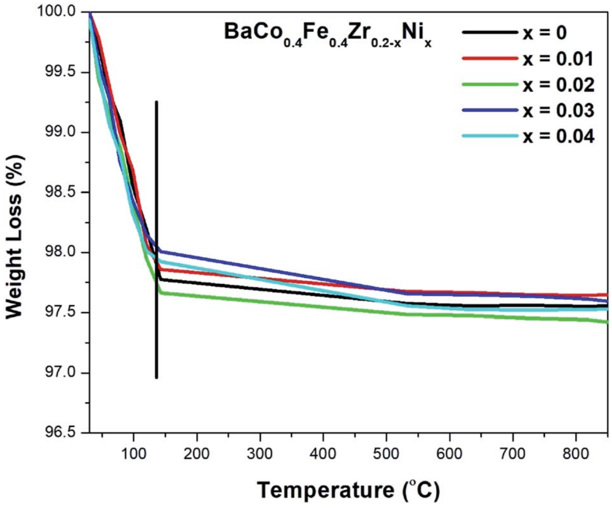

Fig. 5 Thermogravimetric analysis (TGA) curves of $BaCo_{0.4}Fe_{0.4}Zr_{0.2-x}Ni_xO_{3-\delta}$.

electrolyte, and electronic conductivity increases at electrodes. Therefore, $BaCo_{0.4}Fe_{0.4}Zr_{0.2-x}Ni_xO_{3-\delta}$ ($x = 0.04$) exhibited better conductivity compared to other compositions. The high concentration of nickel ($x = 0.04$) resulted in increased electronic defects and increased grain size, thus forcing the electron to transfer from one grain to another through conduction hopping.[50] It can also be deduced that increased grain size leads to the oxygen permeation flux which caused the faster rate of diffusion of oxygen ions by grain boundaries thus enhancing the surface reaction rate. The activation energy for ranges from 0.26–0.27 eV which is comparable to the cathode materials sintered at higher temperature. The low activation energy makes $BaCo_{0.4}Fe_{0.4}Zr_{0.2-x}Ni_xO_{3-\delta}$ cathode suitable for intermediate temperature SOFC. Moreover, activation energy is also linked directly to the grain growth.[51] The obtained conductivity for the nickel BCFZ sintered at low temperature 1200 °C is much better than because nickel acted as sintering aid.

Table 1 Crystalline Size of $BaCo_{0.4}Fe_{0.4}Zr_{0.2-x}Ni_xO_{3-\delta}$

Cathode materials ($BaCo_{0.4}Fe_{0.4}Zr_{0.2-x}Ni_xO_{3-\delta}$)	$x = 0$	$x = 0.01$	$x = 0.02$	$x = 0.03$	$x = 0.04$
Crystallite size (nm)	32	34	42	45	60

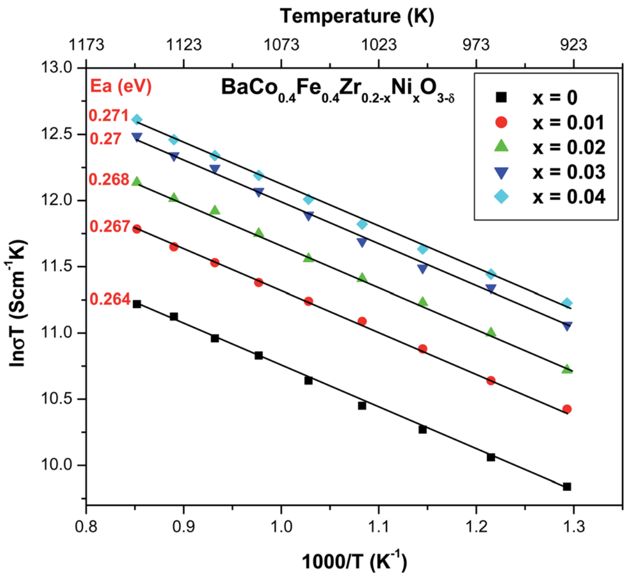

Fig. 6 Arrhenius plot of $BaCo_{0.4}Fe_{0.4}Zr_{0.2-x}Ni_xO_{3-\delta}$.

4 Electrochemical performance

The electrochemical performance of five button cells having configuration ($BaCo_{0.4}Fe_{0.4}Zr_{0.2-x}Ni_xO_{3-\delta}$/SDC/Ni-SDC) is evaluated at temperatures 600 °C, 500 °C and 400 °C. Fig. 7(a–c) gives the *I–V* and power density curves of button cells. It can be observed that the maximum power density of 0.47 W m^{-2} was observed for perovskite cathode material having nickel composition ($x = 0.02$) at 600 °C and OCV of 0.86 V. The power density observed for cells having cathode with concentration ($x = 0, 0.01, 0.03, 0.04$) were 0.29 W m^{-2}, 0.31 W m^{-2}, 0.40 W m^{-2} and 0.34 W m^{-2}. The similar pattern is observed at 500 °C and 400 °C *i.e.* cells having cathode with nickel composition ($x = 0.02$) exhibited maximum power density while minimum power density is observed for composition ($x = 0$).

It was evident from SEM micrographs that cathode material with nickel concentration ($x = 0.02$) had moderate porosity and well-networked structure compared to other compositions therefore cell with a cathode having a nickel composition ($x = 0.02$) exhibit good performance compared to other cells. It can also be observed although cathode ($x = 0.04$) had the highest electronic conductivity compared to other compositions, but due to its dense structure, lesser gas diffusion occurred therefore reduced the oxygen reduction reaction at the cathode and decreasing its electrochemical performance.[24] The obtained electrochemical performance confirms that $BaCo_{0.4}Fe_{0.4}Zr_{0.2-x}Ni_xO_{3-\delta}$ ($x = 0.02$) perovskite cathode material is the best composition at low sintering temperature that can be used as suitable cathode material for application in IT-SOFCs.

Based on the better electrochemical performance of cell having composition ($x = 0.02$), its stability is observed for the 10 hour operation shown in Fig. 8. It can be observed that the cell has shown no apparent degradation with the passage of time at

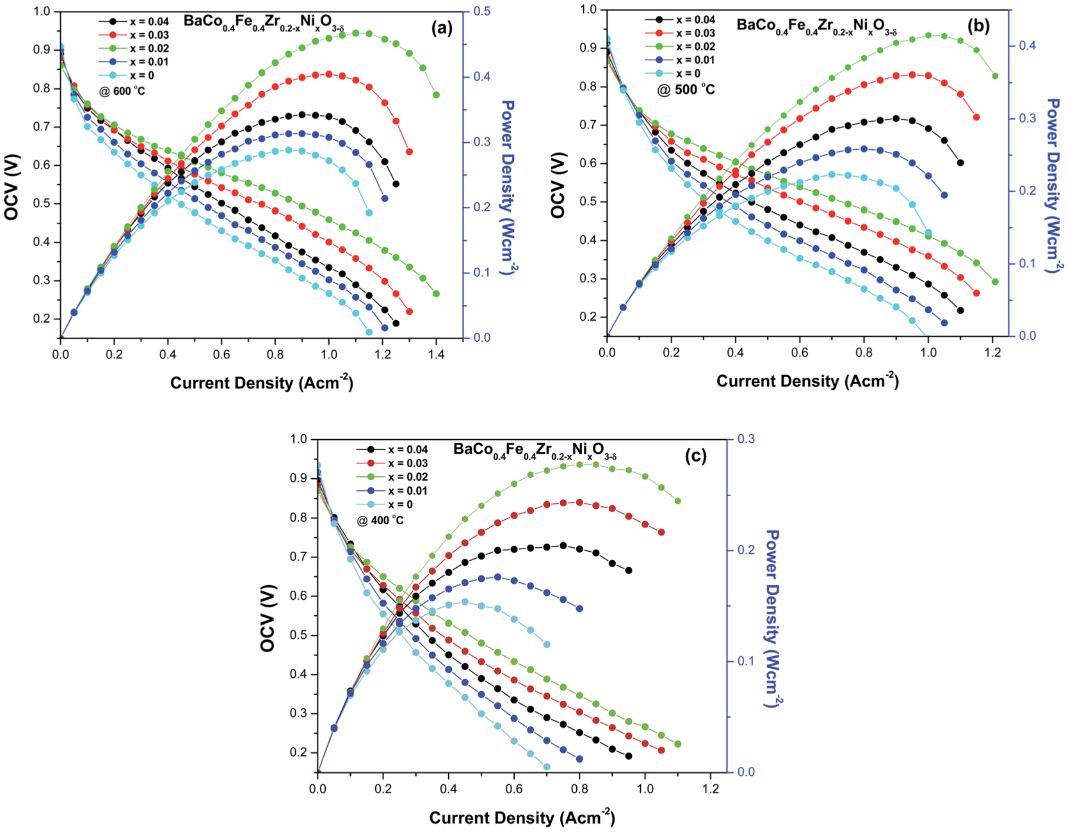

Fig. 7 (a–c) Electrochemical performance of $BaCo_{0.4}Fe_{0.4}Zr_{0.2-x}Ni_xO_{3-\delta}$.

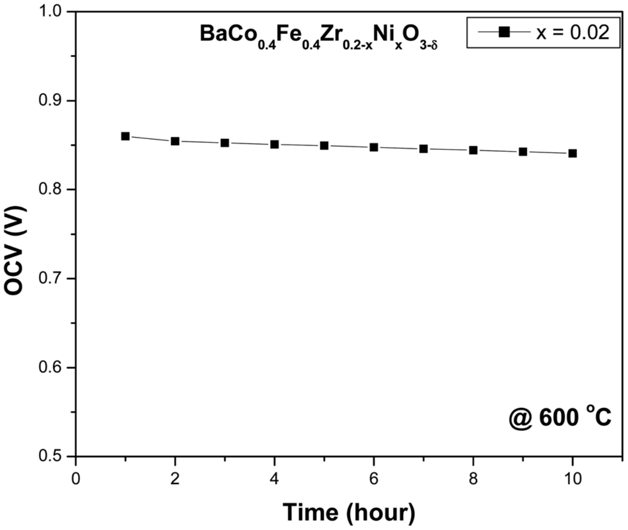

Fig. 8 Stability of $BaCo_{0.4}Fe_{0.4}Zr_{0.2-x}Ni_xO_{3-\delta}$ ($x = 0.02$) cell.

intermediate temperature. The addition of nickel as sintering in cathode will not have significant effect on degradation of cell performance because unlike anode where hydrocarbon is fed which significantly decreases the performance of cell due to carbon coking or sulphur poisoning, air or oxygen is fed at cathode.

5 Conclusion

The $BaCo_{0.4}Fe_{0.4}Zr_{0.2-x}Ni_x$ perovskite cathode material using nickel as sintering aid was successfully synthesized using a cost-effective auto combustion method. $BaCo_{0.4}Fe_{0.4}Zr_{0.2-x}Ni_xO_{3-\delta}$ showed improved sinterability and conductivity at low sintering temperature (1200 °C) with nickel as a sintering aid. Morphological studies confirmed that densification steadily with increased content of nickel and $BaCo_{0.4}Fe_{0.4}Zr_{0.2-x}Ni_xO_{3-\delta}$ ($x = 0.04$) exhibited denser structure compared to other compositions. From structural analysis, increased crystallite size was observed with increased concentration of nickel content and presence of a secondary phase of BaO was attributed to lower sintering. Thermal stability within the SOFC operating temperature range was observed for all compositions. The highest conductivity of $BaCo_{0.4}Fe_{0.4}Zr_{0.2-x}Ni_xO_{3-\delta}$ ($x = 0.04$) was attributed to increased grain size and electronic defects that resulted in the enhanced surface reduction reaction. The peak power density of 0.47 W cm^{-2} was obtained for a cell having $BaCo_{0.4}Fe_{0.4}Zr_{0.2-x}Ni_x$ ($x = 0.02$) cathode at 600 °C, due to its moderate porosity compared to other composition that led to better diffusion of gas and increased electrochemical reaction at the TPB. Therefore, $BaCo_{0.4}Fe_{0.4}Zr_{0.2-x}Ni_xO_{3-\delta}$ perovskite cathode material with the composition ($x = 0.02$) sintered at a sintering temperature of 1200 °C can be a promising candidate for IT-SOFC.

Conflicts of interest

There are no conflicts to declare.

Acknowledgements

We would like to acknowledge Laser and Optronics Center (Department of Physics), UET, Lahore, Pakistan for their support.

References

1 M. Irshad, *et al.*, Evaluation of $BaZr_{0.8}X_{0.2}$ (X = Y, Gd, Sm) proton conducting electrolytes sintered at low temperature for IT-SOFC synthesized by cost effective combustion method, *J. Alloys Compd.*, 2020, **815**, 152389.

2 M. Benamira, L. Thommy, F. Moser, O. Joubert and M. T. Caldes, New anode materials for IT-SOFC derived from the electrolyte $BaIn_{0.3}Ti_{0.7}O_{2.85}$ by lanthanum and manganese doping, *Solid State Ionics*, 2014, **265**, 38–45.

3 M. Irshad, *et al.*, Electrochemical evaluation of mixed ionic electronic perovskite cathode $LaNi_{1-x}Co_xO_{3-\delta}$ for IT-SOFC synthesized by high temperature decomposition, *Int. J. Hydrogen Energy*, 2021, **46**(17), 10448–10456.

4 M. Benamira, *et al.*, Structural and Electrical Properties of Gadolinia-doped Ceria Mixed with Alkali Earth Carbonates for SOFC Applications, *ECS Trans.*, 2019, **7**(1), 2261–2268.

5 M. Irshad, *et al.*, Evaluation of densification effects on the properties of 8 mol% yttria stabilized zirconia electrolyte synthesized by cost effective coprecipitation route, *Ceram. Int.*, 2021, **47**(2), 2857–2863.

6 D. K. Niakolas, M. Daletou, S. G. Neophytides and C. G. Vayenas, Fuel cells are a commercially viable alternative for the production of 'clean' energy, *Ambio*, 2016, **45**(1), 32–37.

7 M. Irshad, *et al.*, A Brief Description of High Temperature Solid Oxide Fuel Cell's Operation, Materials, Design, Fabrication Technologies and Performance, *Appl. Sci.*, Mar. 2016, **6**(3), 75.

8 M. Benamira, *et al.*, Enhancing oxygen reduction reaction of $YSZ/La_2NiO_{4+\delta}$ using an ultrathin $La_2NiO_{4+\delta}$ interfacial layer, *J. Alloys Compd.*, 2018, **746**, 413–420.

9 F. Ramadhani, M. A. Hussain, H. Mokhlis and S. Hajimolana, Optimization strategies for Solid Oxide Fuel Cell (SOFC) application: A literature survey, *Renewable Sustainable Energy Rev.*, 2017, **76**, 460–484.

10 A. M. Abdalla, *et al.*, Nanomaterials for solid oxide fuel cells: A review, *Renewable Sustainable Energy Rev.*, 2018, **82**, 353–368.

11 L. Yang, Z. Liu, S. Wang, Y. Choi, C. Zuo and M. Liu, A mixed proton, oxygen ion, and electron conducting cathode for SOFCs based on oxide proton conductors, *J. Power Sources*, 2010, **195**(2), 471–474.

12 A. Endo, Cathodic reaction mechanism of dense $La_{0.6}Sr_{0.4}CoO_3$ and $La_{0.81}Sr_{0.09}MnO_3$ electrodes for solid oxide fuel cells, *Solid State Ionics*, 2000, **135**(1–4), 353–358.

13 S. Imashuku, T. Uda, Y. Nose, G. Taniguchi, Y. Ito and Y. Awakura, Dependence of Dopant Cations on Microstructure and Proton Conductivity of Barium Zirconate, *J. Electrochem. Soc.*, 2009, **156**(1), B1.

14 J. Sunarso, S. S. Hashim, N. Zhu and W. Zhou, Perovskite oxides applications in high temperature oxygen separation, solid oxide fuel cell and membrane reactor: a review, *Prog. Energy Combust. Sci.*, 2017, **61**, 57–77.

15 M. Burriel, G. Garcia, J. Santiso, J. A. Kilner, R. J. Chater and S. J. Skinner, Anisotropic oxygen diffusion properties in epitaxial thin films of $La_2NiO_{4+\delta}$, *J. Mater. Chem.*, 2008, **18**(4), 416–422.

16 G. J. la O, R. F. Savinell and Y. Shao-Horn, Activity Enhancement of Dense Strontium-Doped Lanthanum Manganite Thin Films under Cathodic Polarization: A Combined AES and XPS Study, *J. Electrochem. Soc.*, 2009, **156**(6), B771.

17 N. Mahato, A. Banerjee, A. Gupta, S. Omar and K. Balani, Progress in material selection for solid oxide fuel cell technology: A review, *Prog. Mater. Sci.*, 2015, **72**, 141–337.

18 K.-Y. Park, Y. Seo, K. B. Kim, S.-J. Song, B. Park and J.-Y. Park, Enhanced proton conductivity of yttrium-doped barium zirconate with sinterability in protonic ceramic fuel cells, *J. Alloys Compd.*, 2015, **639**, 435–444.

19 A. Weber and E. Ivers-Tiffée, Materials and concepts for solid oxide fuel cells (SOFCs) in stationary and mobile applications, *J. Power Sources*, 2004, **127**(1–2), 273–283.

20 N. Laosiripojana, W. Wiyaratn, W. Kiatkittipong, A. Arpornwichanop, A. Soottitantawat and S. Assabumrungrat, Reviews on Solid Oxide Fuel Cell Technology, *Eng. J.*, Feb. 2009, **13**(1), 65–84.

21 S. Hossain, *et al.*, Highly dense and chemically stable proton conducting electrolyte sintered at 1200 °C, *Int. J. Hydrogen Energy*, 2018, **43**(2), 894–907.

22 C. Sun, R. Hui and J. Roller, Cathode materials for solid oxide fuel cells: a review, *J. Solid State Electrochem.*, 2010, **14**(7), 1125–1144.

23 B. B. Panigrahi, N. S. Reddy, A. Balakrishnan, M. C. Chu, S. J. Cho and J. J. Gracio, Nickel assisted sintering of Ti_3SiC_2 powder under pressureless conditions, *J. Alloys Compd.*, 2010, **505**(1), 337–342.

24 T. Kida, A. Yamasaki, K. Watanabe, N. Yamazoe and K. Shimanoe, Oxygen-permeable membranes based on partially B-site substituted $BaFe_{1-y}MyO_{3-\delta}$ (M = Cu or Ni), *J. Solid State Chem.*, 2010, **183**(10), 2426–2431.

25 B. Wang, L. Bi and X. S. Zhao, Exploring the role of NiO as a sintering aid in $BaZr_{0.1}Ce_{0.7}Y_{0.2}O_{3-\delta}$ electrolyte for proton-conducting solid oxide fuel cells, *J. Power Sources*, 2018, **399**, 207–214.

26 Y.-L. Huang, A. M. Hussain, C. Pellegrinelli, C. Xiong and E. D. Wachsman, Chromium Poisoning Effects on Surface Exchange Kinetics of $La_{0.6}Sr_{0.4}Co_{0.2}Fe_{0.8}O_{3-\delta}$, *ACS Appl. Mater. Interfaces*, 2017, **9**(19), 16660–16668.

27 E. Omari, S. Makhloufi and M. Omari, Preparation by Sol–Gel Method and Characterization of Co-doped $LaNiO_3$ Perovskite, *J. Inorg. Organomet. Polym. Mater.*, 2017, **27**(5), 1466–1472.

28 J. S. A. Carneiro, R. A. Brocca, M. L. R. S. Lucena and E. Nikolla, Optimizing cathode materials for intermediate-temperature solid oxide fuel cells (SOFCs): Oxygen reduction on nanostructured lanthanum nickelate oxides, *Appl. Catal., B*, 2017, **200**, 106–113.

29 B. Babu, C. V. Reddy, J. Shim, R. V. S. S. N. Ravikumar and J. Park, Effect of cobalt concentration on morphology of Co-doped SnO_2 nanostructures synthesized by solution combustion method, *J. Mater. Sci.: Mater. Electron.*, 2016, **27**(5), 5197–5203.

30 J. R. Smith, *et al.*, Evaluation of the relationship between cathode microstructure and electrochemical behavior for SOFCs, *Solid State Ionics*, 2009, **180**(1), 90–98.

31 X. Lu, Y. Ding and Y. Chen, $Ba_{0.5}Sr_{0.5}Zn0.2Fe_{0.8}O_{3-\delta}$–$BaCe_{0.5}Zr_{0.3}Y_{0.16}Zn_{0.04}O_{3-\delta}$ composite cathode for proton-conducting solid oxide fuel cells, *J. Alloys Compd.*, 2009, **484**(1–2), 856–859.

32 Y. Yamazaki, R. Hernandez-Sanchez and S. M. Haile, High Total Proton Conductivity in Large-Grained Yttrium-Doped Barium Zirconate, *Chem. Mater.*, 2009, **21**(13), 2755–2762.

33 M. Mamivand, M. A. Zaeem, H. El Kadiri and L. Q. Chen, Phase field modeling of the tetragonal-to-monoclinic phase transformation in zirconia, *Acta Mater.*, 2013, **61**(14), 5223–5235.

34 F. Shen and K. Lu, Perovskite-type $La_{0.6}Sr_{0.4}Co_{0.2}Fe_{0.8}O_3$, $Ba_{0.5}Sr_{0.5}Co_{0.2}Fe_{0.8}O_3$, and $Sm_{0.5}Sr_{0.5}Co_{0.2}Fe_{0.8}O_3$ cathode materials and their chromium poisoning for solid oxide fuel cells, *Electrochim. Acta*, 2016, **211**, 445–452.

35 L. Gao, *et al.*, Antimony-doped $Bi_{0.5}Sr_{0.5}FeO_{3-\delta}$ as a novel Fe-based oxygen reduction electrocatalyst for solid oxide fuel cells below 600 °C, *J. Mater. Chem. A*, 2018, **6**(31), 15221–15229.

36 F. Liang, Z. Wang, Z. Wang, J. Mao and J. Sunarso, Electrochemical Performance of Cobalt-Free Nb and Ta Co-Doped Perovskite Cathodes for Intermediate-Temperature Solid Oxide Fuel Cells, *ChemElectroChem*, 2017, **4**(9), 2366–2372.

37 L. Gao, M. Zhu, T. Xia, Q. Li, T. Li and H. Zhao, Ni-doped $BaFeO_{3-}$ perovskite oxide as highly active cathode electrocatalyst for intermediate-temperature solid oxide fuel cells, *Electrochim. Acta*, 2018, **289**, 428–436.

38 Y. Xia, *et al.*, A novel cobalt-free cathode with triple-conduction for proton-conducting solid oxide fuel cells with unprecedented performance, *J. Mater. Chem. A*, 2019, **7**(27), 16136–16148.

39 M. Qian and G. B. Schaffer, Sintering of aluminium and its alloys, in *Sintering of Advanced Materials*, Elsevier, 2010, pp. 291–323.

40 X. Jiang, F. Wu and H. Wang, Yb-Doped $BaCeO_3$ and Its Composite Electrolyte for Intermediate-Temperature Solid Oxide Fuel Cells, *Materials*, 2019, **12**(5), 739.

41 N. Madoui and M. Omari, Synthesis and Electrochemical Properties of $LaCr_{1-x}Co_xO_3$ ($0 \leq x \leq 0.5$) *via* Co-precipitation Method, *J. Inorg. Organomet. Polym. Mater.*, 2016, **26**(5), 1005–1013.

42 S. M. de Lima and J. M. Assaf, Synthesis and Characterization of $LaNiO_3$, $LaNi_{(1-x)}Fe_xO_3$ and $LaNi_{(1-x)}Co_xO_3$ Perovskite Oxides for Catalysis Application, *Mater. Res.*, 2002, **5**(3), 329–335.

43 S. Tao and J. T. S. Irvine, Conductivity studies of dense yttrium-doped $BaZrO_3$ sintered at 1325 °C, *J. Solid State Chem.*, 2007, **180**(12), 3493–3503.

44 E. Gilardi, *et al.*, Effect of Dopant–Host Ionic Radii Mismatch on Acceptor-Doped Barium Zirconate Microstructure and Proton Conductivity, *J. Phys. Chem. C*, 2017, **121**(18), 9739–9747.

45 A. A. Shah, S. Ahmad and A. Azam, Investigation of structural, optical, dielectric and magnetic properties of $LaNiO_3$ and $LaNi_{1-x}M_xO_3$ (M = Fe, Cr & Co; $x = 5\%$) nanoparticles, *J. Magn. Magn. Mater.*, 2020, **494**, 165812.

46 Y.-P. Fu, H.-C. Wang and J. Ouyang, Electrical conduction behaviors and mechanical properties of Cu doping on B-site of $(La_{0.8}Ca_{0.2})(Cr_{0.9}Co_{0.1})O_{3-\delta}$ interconnect materials for SOFCs, *Int. J. Hydrogen Energy*, 2011, **36**(20), 13073–13082.

47 C. Nityanand, W. B. Nalin, B. S. Rajkumar and C. M. Chandra, Synthesis and physicochemical characterization of nanocrystalline cobalt doped lanthanum strontium ferrite, *Solid State Sci.*, 2011, **13**(5), 1022–1030.

48 R. V. Wandekar, B. N. Wani and S. R. Bharadwaj, Crystal structure, electrical conductivity, thermal expansion and compatibility studies of Co-substituted lanthanum strontium manganite system, *Solid State Sci.*, 2009, **11**(1), 240–250.

49 Z. Wang, *et al.*, A high performance cathode for proton conducting solid oxide fuel cells, *J. Mater. Chem. A*, 2015, **3**(16), 8405–8412.

50 M. A. Siddiqui, V. S. Chandel, M. Shariq and A. Azam, Dielectric and spectroscopic analysis of cobalt doped potassium hexatitanate ($K_2Ti_6O_{13}$) ceramics, *Mater. Sci.*, 2013, **31**(4), 555–560.

51 M. Shang, J. Tong and R. O'Hayre, A promising cathode for intermediate temperature protonic ceramic fuel cells: $BaCo_{0.4}Fe_{0.4}Zr_{0.2}O_{3-\delta}$, *RSC Adv.*, 2013, **3**(36), 15769.